ACS Chemical Neuroscience

Research Article

pubs.acs.org/chemneuro

Identification of a Novel Indoline Derivative for in Vivo Fluorescent Imaging of Blood-Brain Barrier Disruption in Animal Models

Yuhei Nishimura,[†,‡,§,∥,#] Kenichiro Yata,[⊥] Tsuyoshi Nomoto,[▽] Tomoaki Ogiwara,[†] Kohei Watanabe,[▽] Taichi Shintou,[▽] Akira Tsuboyama,[▽] Mie Okano,[▽] Noriko Umemoto,[†] Zi Zhang,[†] Miko Kawabata,[†] Beibei Zhang,[†] Junya Kuroyanagi,[†] Yasuhito Shimada,[†,‡,§,∥] Takeshi Miyazaki,[▽] Takeshi Imamura,[▽] Hidekazu Tomimoto,[⊥,#] and Toshio Tanaka*[,†,‡,§,∥,#]

[†]Department of Molecular and Cellular Pharmacology, Pharmacogenomics and Pharmacoinformatics, Mie University Graduate School of Medicine, Tsu, Mie 514-8507, Japan

[‡]Mie University Medical Zebrafish Research Center, Tsu, Mie 514-8507, Japan

[§]Department of Omics Medicine, Mie University Industrial Technology Innovation Institute, Tsu, Mie 514-8507, Japan

[∥]Department of Bioinformatics, Mie University Life Science Research Center, Tsu, Mie 514-8507, Japan

[⊥]Department of Neurology, Mie University Graduate School of Medicine, Tsu, Mie 514-8507, Japan

[#]Mie University Brain Science and Animal Model Research Center, Tsu, Mie 514-8507, Japan

[▽]Corporate R&D Headquarters, Canon Inc., Ohta-ku, Tokyo 146-8501, Japan

Supporting Information

ABSTRACT: Disruption of the blood-brain barrier (BBB) can occur in various pathophysiological conditions. Administration of extraneous tracers that can pass the disrupted, but not the intact, BBB and detection of the extravasation have been widely used to assess BBB disruption in animal models. Although several fluorescent tracers have been successfully used, the administration of these tracers basically requires intravascular injection, which can be laborious when using small animals such as zebrafish. To identify fluorescent tracers that could be easily administered into various animal models and visualize the BBB disruption *in vivo*, we prepared nine structurally related indoline derivatives (IDs) as a minimum set of diverse fluorescent compounds. We found that one ID, ZMB741, had the highest affinity for serum albumin and emitted the strongest fluorescence in the presence of serum albumin of the nine IDs tested. The affinity to serum albumin and the fluorescence intensity was superior to those of Evans blue and indocyanine green that have been conventionally used to assess the BBB disruption. We showed that ZMB741 could be administered into zebrafish by static immersion or mice by intraperitoneal injection and visualizes the active disruption of their BBB. These results suggest that ZMB741 can be a convenient and versatile tool for *in vivo* fluorescent imaging of BBB disruption in various animal models. The strategy used in this study can also be applied to diversity-oriented libraries to identify novel fluorescent tracers that may be superior to ZMB741.

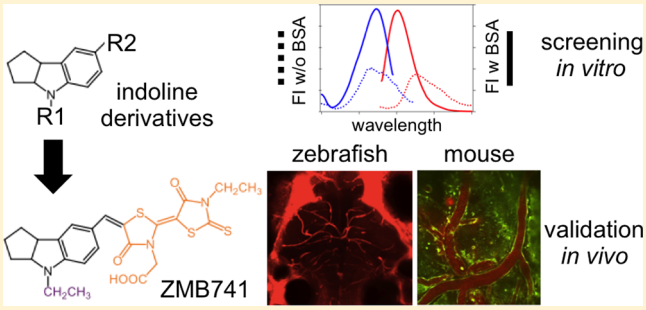

KEYWORDS: *Blood-brain barrier, in vivo fluorescent imaging, low-molecular-weight dyes, diversity-oriented libraries, zebrafish, mouse*

The blood-brain barrier (BBB) is a physiologically dynamic barrier that is important for brain homeostasis and is compromised in diverse pathophysiological conditions, including cerebral ischemia and after exposure to various neurotoxic insults.[1−3] The disruption of the BBB in cerebral ischemia can lead to an extravasation of high-molecular-weight (HMW) molecules such as serum albumin, which draws out water and results in brain edema that is the major cause of mortality following stroke and hemorrhagic transformation.[1,2] BBB disruption during developmental stages could alter the balance between excitation and inhibition and disturb the network connections in the brain, which may contribute to the pathophysiology of psychiatric disorders.[3]

To identify the molecular mechanisms and to develop effective therapeutic interventions targeting BBB disruption, it is important to develop reliable and convenient methods that can assess BBB disruption in various animal models. One global standard is to use tracer molecules that can pass the disrupted, but not the intact, BBB.[4,5] These tracer molecules include Evans blue (EB), indocyanine green (ICG), and fluorescent dextran.

Received: January 9, 2013
Accepted: May 13, 2013
Published: May 13, 2013

Table 1. Physicochemical Properties of EB, ICG, ZMC213, and ZMB741

compd	MW[a]	cLogP[b]	K_d[c]	solvent	λEx (nm)[d]	λEm (nm)[e]	FI max (au)[f]
EB	961	−17.66	2.6	PBS	621	671	6
				PBS with BSA	631	661	1112
ICG	775	−0.29[g]	11	PBS	795	810	816
				PBS with BSA	821	827	4495
ZMC213	389	3.25	13	PBS	525	602	43
				PBS with BSA	518	570	8819
ZMB741	516	3.64	0.5	PBS	523	639	23
				PBS with BSA	546	602	9494

[a]MW: molecular weight. [b]cLogP: calculated octanol/water partition coefficient. [c]K_d: dissociation constant to BSA (μM). [d]λEx: maximum fluorescence excitation. [e]λEm: maximum fluorescence emission. [f]FI max: maximum fluorescence intensity. [g]logP from PubChem database.

EB is a low-molecular-weight (LMW) fluorescent dye (MW: 961 Da) that has a very high affinity to serum albumin.[6] When EB is injected into the bloodstream, it rapidly binds to plasma albumin (MW: 68 kDa), which does not cross the intact BBB. When the BBB is disrupted, the EB−albumin complex leaks into the surrounding brain parenchyma. The extravasation of EB can be visualized by in situ imaging of the brain section.[7−9] EB extravasated into the brain parenchyma can be extracted from brain tissues and quantitatively measured by routine spectrophotometry or fluorescence spectrophotometry.[8] Although EB can be administered into animals by intravenous or intraperitoneal injection,[10] the assessment of BBB disruption using EB requires sacrificing the animals. Therefore, it is impossible to assess the change in BBB disruption during various pathological states or responses to therapeutic interventions in the same animal.

ICG is also a LMW dye (MW: 775 Da) that has a high affinity to serum albumin and emits near-infrared fluorescence.[11] Therefore, the ICG−albumin complex that extravasates from the disrupted BBB into the brain parenchyma at a deep level can be visualized using near-infrared spectroscopy (NIRS) in living animals.[12] However, the resolution of NIRS is relatively low (1−2 mm),[5] making it difficult to apply near-infrared dyes for the assessment of the BBB disruption in small animals such as zebrafish.

High-molecular-weight (HMW) dextran conjugated with a fluorescent small molecule such as fluorescein isothiocyanate or TexasRed has also been used to assess the BBB disruption.[9,13] Fluorescent dextrans can be obtained in different MW (from 3 to 2000 kDa), which allows researchers to examine the extent of BBB disruption.[13] Recent development of two-photon laser scanning microscopy (TPLSM) has allowed us to detect the fluorescent dextrans that extravasated from the disrupted BBB up to depths of about 700 μm under the surface of the cortex of living animal.[14,15] However, because of the HMW, these fluorescent dextrans require intravascular injection for the administration, which may be laborious even in an adult mouse.[16]

There is an increasing amount of evidence showing similarities between the zebrafish and the mammalian BBB that indicate that the zebrafish can be a useful animal model for studying the development, maintenance, and disruption of the BBB.[17−19] Zebrafish are small and transparent so it is possible to visualize the cerebral blood vessels (CBV) of living zebrafish using fluorescent tracers and confocal laser scanning microscopy (CLSM). Although the depth observable by CLSM is shorter than that by TPLSM,[14] the size of zebrafish is small, allowing us to visualize almost all CBV of zebrafish larva using CSLM. Some workers injected fluorescent HMW dextran (MW: 2000 kDa) into zebrafish as extraneous markers of BBB disruption.[17] Others generated a transgenic zebrafish line that expresses a vitamin D binding protein fused with the enhanced green fluorescent protein (MW: 78 kDa) as an endogenous tracer for breakdown of the BBB.[18] Both studies analyzed the leakage of these exogenous or endogenous fluorescent macromolecules from the CBV using CLSM and suggested that the endothelial tight junctions at the zebrafish BBB, which regulate the permeation of HMW molecules through the BBB, develop by 3 days post fertilization (dpf).[17,18] Zebrafish are also amenable for large-scale, phenotype-based forward genetic or chemical screening to uncover novel genes and biologically active compounds relevant to the process of interest.[20−22] A forward genetic approach for a leaky BBB phenotype may identify zebrafish mutants that affect the establishment and maintenance of the BBB. A chemical screening for modifying the leaky BBB phenotype may identify compounds that can be used to treat the BBB disruption. To maximize the utility of the zebrafish in drug discovery mode, it is important to develop exogenous fluorescent tracers that can be easily administered and that visualize the BBB disruption in living zebrafish.

The purpose of this study is to develop novel fluorescent LMW dyes that can be administered into zebrafish and mouse by static immersion and intraperitoneal injection, respectively, and to visualize their BBB disruption by *in vivo* fluorescent imaging using CSLM and TPLSM, respectively.

RESULTS AND DISCUSSION

EB and ICG Require Intracardiac Injection to Visualize the Zebrafish CBV. It has been shown that LMW fluorescent tracers that have a high affinity to serum proteins and can emit strong fluorescence in the presence of serum proteins are advantageous for CBV imaging because these tracers are unlikely to extravasate from intact BBB and are able to provide the high-contrast fluorescent imaging of CBV.[23] We first measured the fluorescence properties of EB and ICG (Supporting Information Figure 1A and D) in the absence or presence of BSA (Supporting Information Figure 1B and E). The maximum fluorescence intensity (FI max) of EB in the absence and presence of BSA was 6 and 1112, respectively (Table 1). The FI max of ICG in the absence and presence of BSA was 816 and 4495, respectively (Table 1). The increases of FI in the presence of BSA are consistent with previous reports.[24,25] The maximum excitation and emission wavelength (λEx and λEm) of EB in the absence and presence of BSA were 621/671 and 631/661, respectively. The λEx and λEm of ICG in the absence and presence of BSA were 795/810 and 821/827, respectively. The red-shift of λEm of ICG in the presence of BSA was consistent with a previous study.[26]

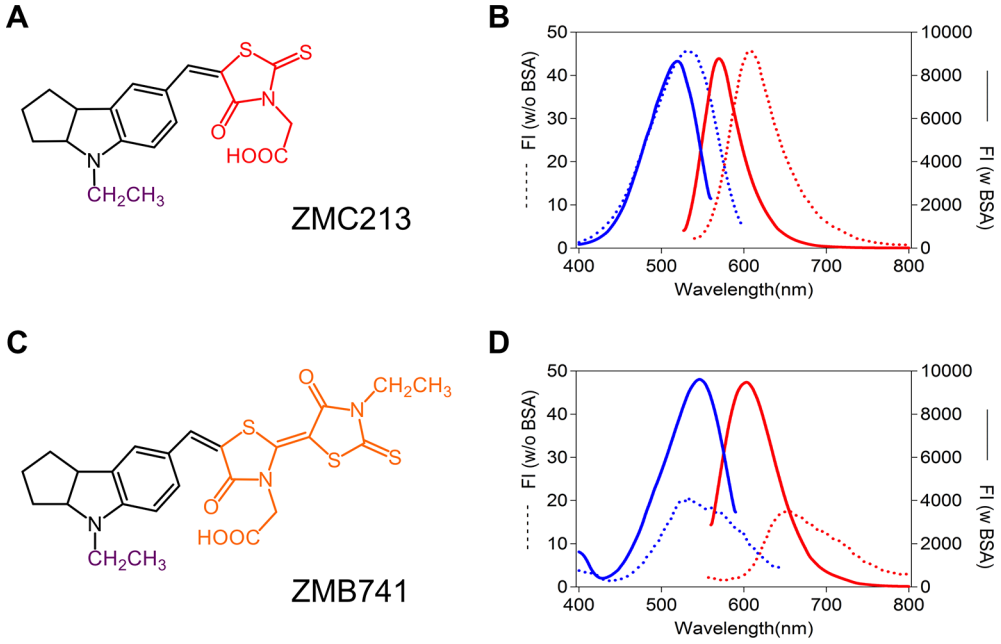

Figure 1. Structures and fluorescence spectra of ZMC213 and ZMB741. (A and C) Structure of ZMC213 (A) and ZMB741 (C). (B and D) Excitation (blue) and emission (red) spectra of ZMC213 (B) and ZMB741 (D) in the absence (dashed line) or presence (solid line) of BSA. In the presence of BSA, the FI max of ZMC213 and ZMB741 increased 206- and 413-fold compared with those in the absence of BSA.

Table 2. Photochemical Properties of ZMC213 and ZMB741 in the Absence and Presence of BSA

		300 K		77 K	300 K	
solvent	compd	Φ_f[a]	τ (s)[b]	τ (s)[b]	k_r (s^{-1})[c]	k_{nr} (s^{-1})[d]
PBS	ZMC213	2.0×10^{-3}		3.9×10^{9}	2.6×10^{8}	1.3×10^{11}
	ZMB741	2.0×10^{-3}		2.4×10^{9}	4.2×10^{8}	2.1×10^{11}
PBS with BSA	ZMC213	2.0×10^{-1}	1.7×10^{9}		1.2×10^{8}	4.7×10^{8}
	ZMB741	2.8×10^{-1}	1.7×10^{9}		1.3×10^{8}	3.3×10^{8}

[a]Φ_f: fluorescence quantum yield. [b]τ: average fluorescence lifetime. [c]k_r: radiative decay constant. [d]k_{nr}: nonradiative decay constant.

The clogP (calculated octanol/water partition coefficient) of EB and logP of ICG are −17.66 and −0.28, suggesting that both EB and ICG are hydrophilic. Although zebrafish have been widely used in large-scale chemical screenings,[20,27] there is increasing evidence showing that hydrophilic chemicals are not absorbed efficiently into zebrafish by static immersion.[27,28] Consistent with this, *in vivo* fluorescent imaging using CLSM of zebrafish stained with EB (100 μM) or ICG (100 μM) by static immersion failed to visualize the CBV (data not shown). We then administered these dyes into zebrafish by intracardiac injection. As shown in Supporting Information Figure 1C and F, both dyes enabled visualization of the CBV. The weak fluorescence observed of ICG may be because of its fluorescence properties. The FI max of ICG was obtained when excited at 821 nm (Table 1), whereas we used a 632 nm laser, being the longest wavelength available in the CLSM.

Based on these results, we hypothesized that LMW dyes that (i) bind to BSA with a high affinity, (ii) emit strong fluorescence in the presence of BSA, (iii) have the FI max that can be obtained using lasers equipped with standard CLSM, and (iv) can be efficiently absorbed into the zebrafish by static immersion could be an important tool for *in vivo* imaging of zebrafish CBV, especially at a screening level.

Identification of ZMC213 and ZMB741 Showing Strong Fluorescence in the Presence of BSA. We have shown that indoline derivatives (IDs) can be efficiently absorbed into zebrafish by static immersion.[19] Others have shown that some ethenyl indoles increase their fluorescence intensity when they bind to BSA.[29] These studies suggest that some IDs can emit strong fluorescence in the presence of BSA, be efficiently absorbed into zebrafish by static immersion, and visualize the CBV of living zebrafish under CLSM. To evaluate the hypothesis, we developed nine IDs (Supporting Information Figure 2). Three IDs were prepared from a common rhodanine ring with an acetic acid group (ZMC213, ZMJ018, and ZMA333). Brother compounds of these IDs were also prepared from two common rhodanine rings with an acetic acid group (ZMB741, ZMA406, and ZMB426). Three IDs of different molecular sizes (ZMC809, ZMB035, and ZMB163) shared one common pyrazole ring.

We then examined the fluorescence spectrum of the nine IDs in the absence or presence of BSA (Supporting Information Figure 3 and Table 1). The FI maxima of these IDs in the absence of BSA (dashed lines) were between 7 (ZMA333) and 43 (ZMC213), which were close to that of EB and much lower than that of ICG (Table 1 and Supporting Information Figure 1). In the presence of BSA, the FI max of IDs having rhodanine ring(s) (ZMC213, ZMJ018, ZMA333, ZMB741, ZMA406, and ZMB426) were over 200-fold higher (solid lines) than those in the absence of BSA. In particular, the increase of FI max of ZMC213 and ZMB741 was 206- and 413-fold, respectively (Figure 1 and Table 1). In contrast, the increase in FI of IDs

dx.doi.org/10.1021/cn400010t | *ACS Chem. Neurosci.* 2013, 4, 1183−1193

having a pyrazole ring (ZMC809, ZMB035, and ZMB163) in the presence of BSA was relatively small (20- to 30-fold). The structure to fluorescence relationships of the nine IDs used in this study suggest that the attachment of a 7-substituted single or double rhodanine ring, but not of a pyrazole one, to indoline may be critical for the interaction of ID with BSA. The relationship also suggests that the attachment of a bulky structure at the N site of indoline scaffold may inhibit the interaction between the ID and BSA.

Photophysical Properties of ZMC213 and ZMB741. To examine the mechanism of the large increase in FI max of ZMC213 and ZMB741 in the presence of BSA (Figure 1 and Table 1), we carried out photophysical measurements and decay kinetic analyses. Table 2 summarizes the photophysical properties of ZMC213 and ZMB741. The fluorescence quantum yields (Φ_f) of ZMC213 and ZMB741 at 300 K in the presence of BSA were 2.0×10^{-1} and 2.8×10^{-1}, respectively, much larger (100- and 140-fold, respectively) than those in the absence of BSA. It has been shown that Φ_f of ICG in plasma was 3.2×10^{-2},[30] suggesting that Φ_f values of ZMC213 and ZMB741 are higher than that of ICG. We then measured the averaged fluorescence lifetime (τ) of ZMC213 and of ZMB741. Since the fluorescence intensities of ZMC213 and ZMB741 in the absence of BSA at 300 K were too weak, the fluorescence lifetime measurements were carried out at 77 K. In the presence of BSA, the fluorescence lifetime measurements were carried out at 300 K. τ values of ZMC213 in the absence and presence of BSA were 3.9 and 1.7 ns, respectively. τ values of ZMB741 in the absence and presence of BSA were 2.4 and 2.2 ns, respectively. Using the measured Φ_f and τ, we calculated the radiative and nonradiative decay rate constants (k_r and k_{nr}, respectively, see Methods). As shown in Table 2, k_r of ZMC213 and ZMB741 were of the same order in both the absence and presence of BSA. In contrast, k_{nr} values of ZMC213 and ZMB741 in the presence of BSA were 272- and 630-fold smaller than those in the absence of BSA. These results suggest that the molecular interaction between ZMC213 or ZMB741 and BSA may effectively suppress the vibrational deactivation in electronic transition from the fluorescent excited state to the ground state, leading to the marked increases in the fluorescence quantum yields in the presence of BSA.

Assessment of Affinity of ZMB741, ZMC213, EB, and ICG to BSA. We then calculated the affinity of EB, ICG, ZMC213, and ZMB741 to BSA based on the fluorescence intensity in the presence of BSA (Supporting Information Figure 4). The K_d values of these fluorescent compounds to BSA were 2.6, 1.1, 1.3, and 0.5 μM for EB, ICG, ZMC213, and ZMB741, respectively (Table 1). The K_d values of EB and ICG are consistent with previous reports.[23,31] These results suggest that ZMB741 has the highest affinity for BSA among the four fluorescent compounds.

It should be noted that the FI max of ZMC213 in the presence of BSA was higher than that of ICG in spite of the higher affinity of ICG to BSA (Table 1). The emission of ICG in the presence of BSA produces a red-shift compared with the emission in the absence of BSA (Table 1). In contrast, there is a blue shift in emission of ZMC213 in the presence of BSA. In general, push−pull type molecules like ICG, EB, and IDs tend to form a fluorescent intramolecular charge-transfer (ICT) excited state.[32] The fluorescence from the ICT state is very sensitive to the environment of the molecules, the solvent polarity, or the nature of the binding site.[32] When the ICT excited state is energetically relaxed in a polar environment, the fluorescence peak shifts to red. Therefore, the red-shift of ICG suggests that the ICG molecule binds to a hydrophilic BSA site with high polarity. On the other hand, ZMC213 binds to a less-polar, hydrophobic BSA site to make the fluorescence peak blue-shift as compared with that in a polar PBS solution. The previous paper[32] showed that the fluorescence quantum yield of the ICT molecule increased with increasing hydrophobicity of its environment. On the basis of the above discussion, it is reasonable that ZMC213, with a lower affinity to BSA than ICG, exhibits substantially higher fluorescence upon binding to BSA.

It has also been shown that the fluorescent ethenyl indole compounds indicated a fluorescence blue-shift and intensity enhancement when binding to BSA.[29] The binding sites of the ethenyl indole on BSA were found to be adjacent to a tryptophan residue, leading to the fluorescence quenching of tryptophan. Similarly, we have also observed fluorescence quenching of a tryptophan residue when IDs (ZMC213 and ZMB741) bound to BSA (data not shown). Therefore, these IDs may bind to BSA at hydrophobic sites adjacent to the tryptophan residue.

The Scatchard analysis (Supporting Information Figure 4) showed smaller x-intercept values (Bmax) than the total concentration of BSA (10 μM). These results suggest the existence of multiple binding sites in BSA, which possess different degrees of fluorescence enhancement of IDs. The determined K_d values of ZMC213 and ZMB741 were much smaller than the concentration of albumin in normal blood (~700 μM). Therefore, it seems that the existence of multiple binding sites does not become a hindrance factor for *in vivo* imaging of BBB disruption.

ZMC213 and ZMB741 Visualized the Zebrafish CBV by Static Immersion. The clogP values of ZMC213 and ZMB741 are 3.25 and 3.64, respectively (Table 1), suggesting these dyes may be efficiently absorbed into zebrafish during static immersion. Therefore, we evaluated the ability of ZMC213 and ZMB741 administered by static immersion to visualize the CBV of living zebrafish using CLSM. The CBV of zebrafish immersed in fish medium containing 10 μM ZMC213 was visualized with excitations at 488 or 543 nm that results in a yellow color in the CBV in the merged image (Figure 2A). In contrast, the CBV of zebrafish immersed in fish medium containing 10 μM ZMB741 was brightly visualized with the excitation at 543 nm but not at 488 nm, resulting in a red color in the CBV in the merged image (Figure 2B).

The maximum emission of ZMC213 was at 525 nm in the absence of BSA and 518 nm in the presence of BSA. In contrast, the maximum emission of ZMB741 was at 523 nm in the absence of BSA and 546 nm in the presence of BSA. Although it is currently unknown why the maximum emissions of ZMC213 and ZMB741 showed the blue- and red-shift, respectively, in the presence of BSA, the difference can explain why ZMC213 but not ZMB741 can be efficiently excited at 488 nm. The selectivity of ZMB741 is advantageous especially when using transgenic zebrafish lines expressing the green fluorescent protein in specific tissues or cells. There were no obvious extravasations of these dyes from the CBV, suggesting that these dyes do not pass across the intact BBB.

We selected ZMB741 because it showed the strongest FI in the presence of BSA and the highest affinity to BSA (Table 1), the highest Φ_f in the presence of BSA (Table 2), and the selective fluorescence excited at 543 nm but not 488 nm

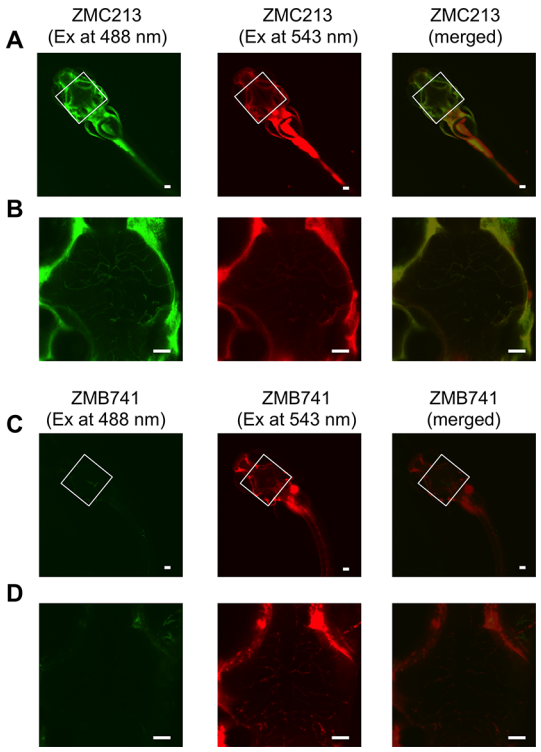

Figure 2. *In vivo* fluorescent imaging of CBV of zebrafish using ZMC213 or ZMB741 administered by static immersion. Zebrafish larvae at 8 dpf were immersed in fish medium containing 10 μM ZMC213 (A and B) or ZMB741 (C and D) for 3 h. *In vivo* fluorescence imaging of the zebrafish was performed using CLSM with excitation at 488 or 543 nm. (A) and (C) were taken with a 5× objective lens. (B) and (D) were taken with a 20× objective lens for the area indicated by white rectangles in (A) and (C). Scale bar: 50 μm.

(Figure 2). Next we tested its ability for *in vivo* imaging of BBB disruption using animal models.

ZMB741 Visualized BBB Disruption in Zebrafish Exposed to Lead Acetate. To examine whether ZMB741 could visualize BBB disruption in zebrafish, we exposed zebrafish to lead acetate (PbAc) during development. Exposure to lead during developmental stages can cause BBB disruption in mammals, at least partly through the reduction of tight junction proteins between the endothelial cells.[33,34] *In vivo* fluorescent imaging of the CBV were performed using zebrafish stained with EB administered by intracardiac injection or ZMB741 administered by static immersion. Extravasations of both EB (Figure 3A) and ZMB741 (Figure 3C) in zebrafish exposed to PbAc were clearly visualized but not in zebrafish without PbAc. Quantitative analysis of these *in vivo* fluorescent imaging revealed that the ratios of FI in the brain parenchyma to FI in the CBV of zebrafish exposed to PbAc was higher than those of zebrafish without exposure of PbAc for both EB (Figure 3B) and ZMB741 (Figure 3D). In zebrafish stained with EB, the average ratio of FI in zebrafish exposed to PbAc was 142% of that of zebrafish without exposure to PbAc (p = 0.05). In zebrafish stained with ZMB741, the average ratio of FI in zebrafish exposed to PbAc was 175% of that of zebrafish without exposure to PbAc (p = 0.002).

Several reasons may explain the superiority of ZMB741. First, ZMB741 can be easily administered by immersion to several zebrafish at a time. In contrast, EB requires intracardiac injection, which is labor intensive and technically difficult in zebrafish, resulting in relatively few zebrafish able to be used for *in vivo* fluorescent imaging. Because the sample size affects the statistical power, the ease of getting many samples is an advantage of ZMB741. Second, because intracardiac injection is invasive, the cardiac function may be impaired and hypoperfusion in CBV may occur. It has been shown that extravasation of tracers from the disrupted BBB can be influenced by the circulation of CBV.[35] Therefore, the extravasation of tracers administered by intracardiac injection

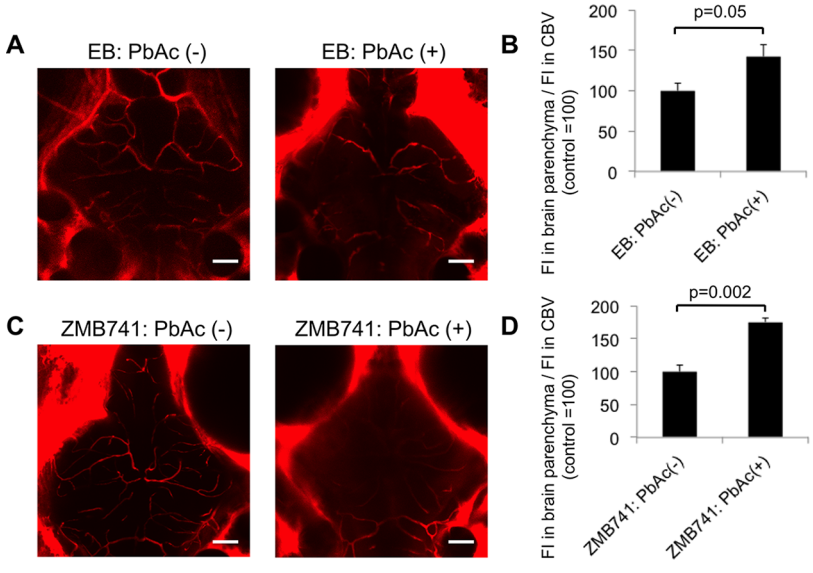

Figure 3. *In vivo* fluorescent imaging of CBV of zebrafish exposed to lead acetate using EB administered by intracardiac injection and ZMB741 administered by static immersion. Zebrafish larvae (7 dpf) with and without exposure to lead acetate (3 μM) from 6 hpf to 7 dpf were stained with EB by intracardiac injection or ZMB741 (5 μM) by static immersion. CLSM was used to obtain *in vivo* fluorescent imaging of the CBV of zebrafish stained with EB by intracardiac injection (A) and ZMB741 by static immersion (C). (B and D) Quantitative analysis of the *in vivo* fluorescent imaging using EB (B, n = 4 for PbAc-, n = 3 for PbAc+) and ZMB741 (D, n = 6 for PbAc-, n = 4 for PbAc+). Scale bar: 50 μm.

dx.doi.org/10.1021/cn400010t | *ACS Chem. Neurosci.* 2013, 4, 1183−1193

may underestimate the BBB disruption. Third, the fluorescent properties are different between EB and ZMB741. Although there are many studies detecting fluorescence of EB using helium−neon laser (543 nm) in CLSM,[9,13] the maximum fluorescence excitation of EB in the presence of albumin was 631 nm, suggesting that the emission of EB may be submaximal with this instrument. In contrast, the maximum fluorescence excitation of ZMB741 in the presence of albumin was 546 nm, close to the maximum of the helium−neon laser, suggesting that ZMB741 can emit maximum fluorescence using CLSM.

ZMB741 Visualized BBB Disruption in Zebrafish Exposed to Proconvulsant. To further validate the utility of ZMB741 in the assessment of BBB disruption in living zebrafish, we applied ZMB741 to zebrafish exposed to pentylenetetrazole (PTZ), a proconvulsant that has been widely used to induce seizures in various animal models including zebrafish.[36] It has been shown that the BBB can be disrupted after seizures induced by PTZ.[37] We exposed zebrafish to PTZ for 2 days and stained the zebrafish with ZMB741 by static immersion. *In vivo* fluorescent imaging of the CBV clearly visualized the extravasation of ZMB741 in zebrafish exposed to PTZ but not in control zebrafish (Figure 4). Quantitative analysis of the *in vivo* imaging revealed that the

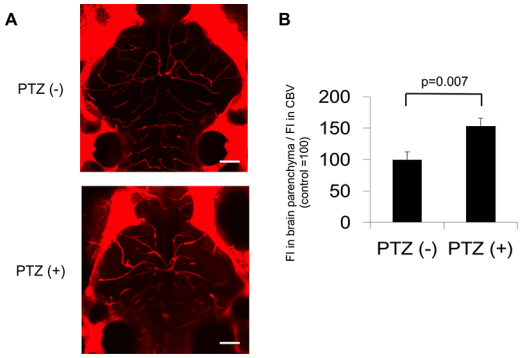

Figure 4. *In vivo* fluorescent imaging of CBV of zebrafish exposed to pentylenetetrazole using ZMB741 administered by static immersion. Zebrafish larvae were exposed to DMSO (0.1%) or pentylenetetrazole (2 mM) from 5 to 7 dpf, followed by the staining with ZMB741 (5 μM) by static immersion for 1 day. After the staining, *in vivo* fluorescent imaging of the CBV was performed using CLSM. (A) *In vivo* fluorescent imaging of the CBV of zebrafish stained with ZMB741 by static immersion. (B) Quantitative analysis of the *in vivo* fluorescent imaging (n = 3 for PTZ- and n = 6 for PTZ+). Scale bar: 50 μm.

ratio of FI in brain parenchyma and CBV in zebrafish exposed to PTZ was significantly higher (p = 0.007) than that of control zebrafish (Figure 4). These results suggest that ZMB741 can be a reliable and convenient tool to assess the BBB disruption in zebrafish.

ZMB741 Visualized the Living Mouse CBV by Intraperitoneal Administration. We then evaluated whether ZMB741 administered into mice by intraperitoneal injection could enable visualization of the mouse CBV using TPLSM. As shown in Figure 5, the fluorescent intensity of in the CBV gradually increased up to 60 min after the intraperitoneal injection then gradually decreased over the next 60 min. ZMB741 did not show obvious extravasation into the mouse brain throughout the whole observation period, suggesting that ZMB741 does not pass across the intact BBB. TexasRed-dextran administered into mouse by intravenous injection also clearly visualized the CBV (Figure 5). The fluorescent intensity in the CBV peaked just after the intravenous injection and gradually decreased for a further 180 min. To examine whether the difference in kinetics could be due to the difference in the administration route, we administered ZMB741 into mouse by intravenous injection (Supporting Information Figure 5). The fluorescent intensity of ZMB741 in the CBV increased just after the intravenous injection, followed by a time-dependent decrease similar to that of TexasRed-dextran. In contrast, TexasRed-dextran administered intraperitoneally into mouse failed to visualize the CBV up to 60 min post injection (Supporting Information Figure 5). These results suggest that ZMB741 can visualize the living mouse CBV by either intravenous or intraperitoneal injection and that the CBV can be visualized for several hours by ZMB741 when administered intraperitoneally.

To further compare the ability of ZMB741 and TexasRed-dextran for *in vivo* imaging of mouse CBV, we used a mouse line expressing GFP under the control of a β-actin promoter.[38] The CBV of the mice were observed using TPLSM following administration of ZMB741 or TexasRed-dextran to mice intraperitoneally or intravenously, respectively. Both visualized the capillary vessels well (Supporting Information Figure 6). Intravenous injection can be difficult when the vein is very narrow or leaky and as the pigmentation and the thickness of the skin increases.[16] In contrast, intraperitoneal injection is very easy and can be performed repeatedly, even in neonatal rodent models. The effectiveness of ZMB741 administered into mouse by intraperitoneal injection can increase the throughput of experiments.

ZM-B741 Visualized BBB Disruption in Mouse Model of Transient Cerebral Ischemia. To examine the ability of ZMB741 to visualize the BBB disruption in a living mouse, we used a transient cerebral ischemia model.[39] The BBB in this ischemia model is disrupted and HMW molecules extravasate from the BBB 1 day after the onset of the ischemia.[40] Preocclusion of bilateral carotid arteries, *in vivo* fluorescent imaging of the mouse CBV revealed no abnormality in the absence or presence of ZMB741 (Figure 6 and Supporting Information Movie 1A). However, 24 h postocclusion, rolling and adhesion of leukocytes in the venules were visualized both in the absence and presence of ZMB741 and the extravasation of ZMB741 from the venules were clearly visualized in the presence of ZMB741 (Figure 6, Supporting Information Movie 1B). The rolling and adhesion of leukocytes in the venules were consistent with previous reports.[41,42] These results suggest that ZMB741 administered by intraperitoneal injection can visualize BBB disruption in a living mouse. The sensitivity of *in vivo* fluorescent imaging of BBB disruption may be lower than that of the in situ imaging such as immunohistochemistry using horseradish peroxidase as a tracer.[43] However, *in vivo* fluorescent markers give more high-throughput imaging than in situ imaging and enable researchers to visualize the change of the integrity of BBB disruption in various pathological state and in response to therapeutic interventions in a same, live animal. *In vivo* fluorescent imaging can complement in situ imaging by identifying the molecular mechanisms and in developing effective therapeutic interventions targeting BBB disruption.

In summary, we identified ZMB741, a novel LMW fluorescent dye as suitable for *in vivo* imaging of BBB disruption in zebrafish and mice. Because of the ease of administration and its strong fluorescence, ZMB741 can be a versatile tool in forward-genetic and chemical screenings to identify genes related to BBB disruption and chemicals for the treatment,

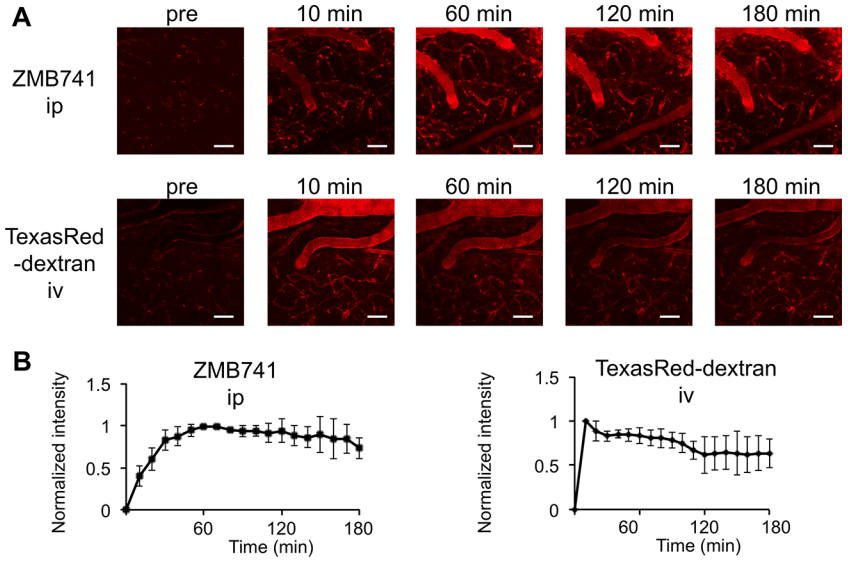

Figure 5. Time-lapse imaging of mouse CBV using ZMB741 and Texas-Red dextran administered by intraperitoneal and intravenous injection, respectively. (A) Mice (10 week old) were used for *in vivo* fluorescent imaging of the CBV using TPSLM with ZMB741 administered by intraperitoneal injection with excitation at 810 nm (upper panels) or TexasRed-dextran administered by intravenous injection with excitation at 910 nm (lower panels). The *in vivo* fluorescent imaging was performed every 10 min. (B) Quantitative analysis of fluorescent intensity in the CBV of mouse using ZMB741 administered by intraperitoneal injection or TexasRed-dextran administered by intravenous injection. Scale bar: 50 μm.

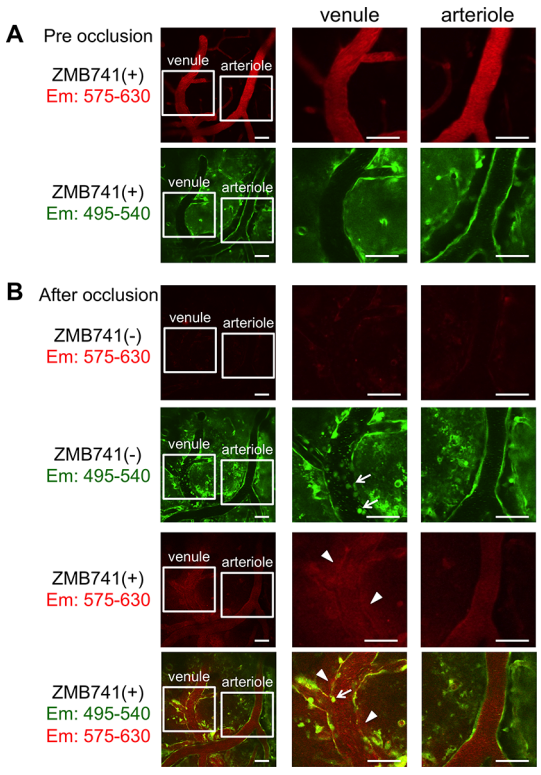

Figure 6. *In vivo* fluorescent imaging of BBB disruption in a mouse model for transient global cerebral ischemia using intraperitoneal injected ZMB741. Both common carotid arteries of green mice (10 weeks old) were exposed and occluded with aneurysm clips for 10 min. After the occlusion, the circulation was restored by removing the clips. *In vivo* fluorescent images of the mouse CBV were taken at preocclusion (A) and 24 h after reperfusion (B) with and without administration of ZMB741. At 24 h after the occlusion, extravasation of ZMB741 from the CBV (arrowhead) and rolling and adhesion of leukocytes (arrow) were clearly visualized in venules but not arterioles. Scale bar: 50 μm.

management, or prevention of the disruption of the BBB. The strategy used in this study can also be applied to diversity-oriented libraries to identify LMW dyes that may be superior to ZMB741.

METHODS

Zebrafish and Mouse Strains. We used a transparent zebrafish mutant line *MieKomachi 001* (*MK001*) that was created by crossing *nacre* [44] and *rose*.[45] *MK001* is also referred to as the *absolute* by the Zebrafish International Resource Center. The zebrafish were bred and maintained according to the methods described by Westerfield[46] with some modification. Briefly, zebrafish were raised at 28.5 ± 0.5 °C with a 14 h/10 h light/dark cycle. Embryos were obtained via natural mating and cultured in fish medium (0.07 mM KCl, 2 mM $CaCl_2$, 0.5 mM $MgSO_4$, and 0.7 mM $NaHCO_3$ at pH 7.4). Mie University Institutional Animal Care and Use Committee have decided that no approval is required to do the experiment using zebrafish. However, the animal experiment in this paper conformed to the ethical guidelines established by the Institutional Animal Care and Use Committee at Mie University.

We also used green fluorescent protein transgenic mice [Green mouse; C57BL/6-Tg (CAG-EGFP) Osb, 8-week old] obtained from Japan SLC, Inc. (Shizuoka, Japan). The experiments using mice were approved by the Institutional Board Committee for Animal Care and Use of Mie University (Permit Number 20-23-rev1).

Compounds. All fluorescent IDs examined in this study (ZMC213, ZMJ018, ZMA333, ZMB741, ZMA406, ZMB428, ZMC809, ZMB035, and ZMB163) were obtained from Canon Inc. (Tokyo, Japan). EB and ICG were purchased from Tokyo Kasei Co. (Tokyo, Japan). BSA (Fraction V, fatty acid-free) was purchased from Calbiochem (La Jolla, CA). Lead acetate and pentylenetetrazole were purchased from Sigma-Aldrich Co. (St. Louis, MO). TexasRed-dextran was purchased from Invitrogen (Grand Island, NY). Stock solutions of chemicals were prepared by dissolving them in dimethyl sulfoxide (DMSO), except for TexasRed-dextran which was dissolved in phosphate buffered saline.

Measurement of Fluorescence Spectrum and Quantum Yield of Fluorescent Compounds. The fluorescence excitation and emission spectra and the fluorescence intensity of these compounds were obtained by measuring 7 μM solutions of the fluorescent compounds in PBS or PBS containing 5% (w/v) BSA with

dx.doi.org/10.1021/cn400010t | *ACS Chem. Neurosci.* 2013, 4, 1183−1193

a FL4500 fluorescence spectrophotometer (Hitachi High-Technologies, Tokyo, Japan). MW and clogP were calculated using ChemDraw 12.0 (CambridgeSoft Corporation, Cambridge, MA).

Fluorescence quantum yields were determined with a reference of fluorescein (Φ_f = 0.88).[47] Fluorescence lifetimes were measured by using a Hamamatsu Photonics C4334 streak scope with excitation lights (371 nm for ZMB741 and 438 nm for ZMC213) from pulse laser diodes (Hamamatsu photonics M8903 series). The decay curves were found to be expressed by a sum of two components:

$$I = A_1 \exp(-t/\tau_1) + A_2 \exp(-t/\tau_2)$$

where τ_n and A_n (n = 1, 2) are the lifetimes and pre-exponential factors, respectively.

Averaged lifetime τ is expressed as

$$\tau = (A_1\tau_1 + A_2\tau_2)/(A_1 + A_2)$$

The radiative and nonradiative rate constants from a fluorescent excited state to a ground state were expressed as the following equations:

$$k_r = \Phi_f/\tau \quad (1)$$

$$k_{nr} = (1 - \Phi_f)/\tau \quad (2)$$

where k_r, k_{nr}, Φ_f, and τ denote radiative and nonradiative rate constant, fluorescence quantum yield and fluorescence lifetime, respectively. The rate constants for the presence of BSA were calculated according to eqs 1 and 2 with use of Φ_f and τ measured at 300 K. In the case without BSA, the rate constants were calculated by using Φ_f at 300 K and τ at 77 K. In the calculation, we assumed that (i) Φ_f = 1.0 at 77 K and (ii) the k_r value was independent of temperature between 77 and 300 K.[48] The former assumption is based on a hypothesis that vibrational deactivation is surely suppressed at 77 K. The latter assumption is based on a hypothesis that k_r could be independent of temperature. With these assumptions, k_r and k_{nr} at 300 K can be described as

$$k_r = 1/\tau(77\ \mathrm{K})$$

$$k_{nr} = k_r(1 - \Phi_f(300\ \mathrm{K}))/\Phi_f(300\ \mathrm{K})$$

Measurement of the Affinity of Fluorescent Compounds for BSA. The quantitation of dissociation constants defining the formation of the chemical species, which cause the fluorescence enhancement in the system that BSA coexists with IDs, were estimated from Scatchard analysis. In the condition that the quantity of BSA is constant (10 μM) and varying quantities of ID coexist, the concentrations of the chemical species ([Dye-BSA]) were determined by fluorometry. The linear calibration curves for each chemical species ([Dye-BSA]) versus fluorescence intensity ratio were preliminarily obtained in the system where an excess amount of BSA (700 μM) coexists with the IDs.

In Vivo Imaging of Zebrafish CBV Using CLSM. For static immersion, zebrafish larvae were immersed in fish medium containing either EB (100 μM), ICG (100 μM), ZMC213 (10 μM), or ZMB741 (10 μM for Figure 2, 5 μM for Figures 3 and 4) at 28.5 °C. After the immersion, zebrafish larvae were washed, anesthetized with 2-phenoxyethanol (500 ppm), and transferred onto glass slides. For intracardiac injection, zebrafish larvae were anesthetized with 2-phenoxyethanol (500 ppm) and mounted lateral side up in 3% low-melting agarose. Microinjection pipettes were made from glass capillaries (1.0 mm diameter, model GD-1, Narishige, Tokyo, Japan) using a vertical puller (model PC-10, Narishige). Solutions of 10 mM EB or ICG in DMSO were loaded into the micropipet, and approximately 1–2 nL (approximately 10–20 pmol) were injected into the heart. After the administration, the zebrafish larvae were transferred onto glass slides. A few drops of 3% low-melting agarose solution were placed over the larvae and the larvae were immediately oriented with dorsal-side-up. The CBV in the embedded larvae were observed using a Zeiss 510 CLSM with a 20× (NA 0.75) objective lens (Carl Zeiss, Oberkochen, Germany) according to previous reports.[19,49] We used 488 nm (argon laser) to detect fluorescence emission from 500 to 530 nm, 543 nm (helium–neon laser) to detect fluorescence emission above 560 nm, and 633 nm (helium–neon laser) to detect fluorescence emission above 650 nm.

Z-Stack imaging (2.4 μm steps) was performed from the depth where left and right mesencephalic central arteries merged (approximately 80 μm below the top of the CBV) to 36 μm above the depth to obtain 15 optical slices. These were used to make a single 256 gray scale (0–255) image using "extended focus" and "capture snapshot" functions of Volocity (Perkin-Elmer, Cambridge, MA). The quantitative assessment of the *in vivo* fluorescent imaging was performed as follows. First, we determined the region of interest (ROI) where the fluorescent intensities in the CBV and brain parenchyma were not saturated (i.e., the maximum fluorescent intensity was below 255). Second, the pixel counts in the CBV and brain parenchyma were calculated using a threshold that could discriminate the CBV and brain parenchyma in the ROI. Third, the pixel counts in the CBV and brain parenchyma were separately integrated by the mean fluorescent intensity in the CBV and brain parenchyma in the ROI. Fourth, the integrated value of the brain parenchyma was divided by that of the CBV to calculate the ratio of fluorescent intensity between the brain parenchyma and the CBV.

In Vivo Imaging of BBB Disruption in Zebrafish Exposed to Lead Acetate. Zebrafish embryos were immersed in the fish medium containing 3 μM lead acetate (PbAc) from 6 h post fertilization (hpf) to 7 dpf. The fish medium was changed every day. At 7 dpf, the zebrafish were immersed in fish medium containing 5 μM of ZMB741 for 3 h or administered with EB by intracardiac injection. *In vivo* imaging of zebrafish CBV using CLSM was performed at 3 h after administration of ZMB741 or EB. Quantification of the *in vivo* fluorescent imaging was performed using Volocity as described above.

In Vivo Imaging of BBB Disruption in Zebrafish Exposed to Pentylenetetrazole. Zebrafish embryos were immersed in the fish medium containing 2 mM pentylenetetrazole from 5 to 7 dpf. At 7 dpf, the zebrafish were immersed in fish medium containing 5 μM of ZMB741 for 1 day and *in vivo* imaging of zebrafish CBV using CLSM and quantification of the *in vivo* fluorescent imaging were performed using Volocity as described above.

In Vivo Imaging of Mouse CBV Using TPLSM. Green mice (10 week old) were anesthetized with isoflurane (3.5% and 1% for induction and maintenance, respectively) in air using a facemask. A rectal probe was inserted into mice to measure the rectal temperature, which was maintained at 37.0 °C with the use of a heating pad. After anesthesia, each mouse was placed in a stereotactic frame and its head immobilized. A 1 × 1 mm^2 cranial window (intact dura) was exposed over the left front parietal cortex as previously described.[50] Plasma-labeling was performed using intravenous injection of 70 kDa TexasRed-dextran (0.7 mg/kg), intraperitoneal injection of 70 kDa TexasRed-dextran (2.1 mg/kg), intraperitoneal injection of ZMB741 (25.8 mg/kg), or intravenous injection of ZMB741 (5 mg/kg). In our experiments, all mice in which ZMB741 was intraperitoneally administered at 25.8 mg/kg have lived without any obvious toxicity, suggesting that any toxicity of ZMB741 intraperitoneally administered into mouse at 25.8 mg/kg can be ignored. After the plasma-labeling, the animal on the stereotactic frame was transferred to the stage of the TPLSM instrument. The TPLSM setup was composed of an upright microscope (BX61WI; Olympus, Tokyo, Japan) and an FV1000-2P laser-scanning microscope system. The excitation source was Ti:sapphire lasers (Mai Tai, Spectra Physics, CA), tuned and mode-locked at 910 nm for TexasRed-Dextran or at 810 nm for ZMB741 and GFP. The emissions of GFP, TexasRed-dextran, and ZMB741 could be separated by a beam splitter (570 nm) and band-pass filters (495–540 nm for GFP and 575–630 nm for TexasRed-dextran and ZMB741). Image stacks of microvasculature were taken with a 20× water immersion objective (1.0 NA). Data were analyzed by Fluoview (Olympus, Tokyo, Japan). For visualization purposes, "maximum intensity projection" was performed for vessel images. Fluorescent signal intensity was measured by averaging all pixel data within a ROI manually selected around the center the microvessels. A mean time–intensity curve was measured and normalized to the peak value in each mouse.

In Vivo Imaging of BBB Disruption in a Mouse Model of Transient Cerebral Ischemia. Transient cerebral ischemia model was made as previously described.[39] Briefly, after making a median incision in the neck skin, both common carotid arteries were exposed and occluded with aneurysm clips for 10 min and then circulation was restored by removing the clips. After intraperitoneal administration of ZMB741, *in vivo* imaging of mouse CBV was performed as described above. The *in vivo* imaging was performed preocclusion and 24 h after reperfusion.

Statistical Analysis. Statistical analysis was performed using SAS version 9.1 (SAS Institute, Cary, NC). Student's *t* test was performed to compare the means of two groups.

■ ASSOCIATED CONTENT

Supporting Information

In vivo imaging of zebrafish CBV using EB and ICG (Supplemental Figure 1), the structures of IDs used in this study (Supplemental Figure 2), the fluorescence spectra of IDs in the absence or presence of BSA (Supplemental Figure 3), scatchard plots of EB, ICG, ZMC213, and ZMB741 for the assessment of affinity to 10 μM BSA (Supplemental Figure 4), *in vivo* fluorescent imaging of mouse CBV using ZMB741 administered by intravenous injection or TexasRed-dextran administered by intraperitoneal injection (Supplemental Figure 5), *in vivo* fluorescent imaging of mouse CBV using ZMB741 or Texas-Red dextran administered by intraperitoneal and intravenous injection, respectively (Supplemental Figure 6), physicochemical properties of EB, ICG, and nine IDs (Supplemental Table 1), and movies for *in vivo* fluorescent imaging of BBB disruption using ZMB741 administered by intraperitoneal injection in a mouse model for transient cerebral ischemia (Supplemental Movie 1). This material is available free of charge via the Internet at http://pubs.acs.org.

■ AUTHOR INFORMATION

Corresponding Author

*Mailing address: Department of Molecular and Cellular Pharmacology, Pharmacogenomics and Pharmacoinformatics, Mie University Graduate School of Medicine, 2-174 Edobashi, Tsu, Mie 514-8507, Japan. Tel: +81-59-231-5411. Fax: +81-59-232-1765. E-mail: tanaka@doc.medic.mie-u.ac.jp.

Author Contributions

YN, KY, and TN contributed equally to this work. YN, KY, and TN conceived the study, carried out the experiments, and wrote the manuscript. TO performed *in vivo* fluorescent imaging of BBB disruption in zebrafish. KW conceived the study and carried out *in vivo* pharmacokinetic validation using zebrafish. TS, AT, and MO performed *in vitro* pharmacodynamics screening. NU, ZZ, MK, BZ, JK, and YS helped to carry out the experiments. TM, TI, and HT conceived the study. TT conceived the study and wrote the manuscript.

Funding

This work was supported, in part, by the New Energy and Industrial Technology Development Organization, Long-range Research Initiative of the Japan Chemical Industrial Association, The Johns Hopkins Center for Alternatives to Animal Testing, and Mie University (COE-B), Grant for Environmental Research by The Sumitomo Foundation, the Ministry of Education, Sports, Science and Culture of Japan, and the Japan Science and Technology Agency.

Notes

The authors declare the following competing financial interest(s): YN, TN, KW, YS, TT were involved in a collaborative contract between Mie University and Canon Inc. under the regulation of Grant for Practical Application of University R&D Results under the Matching Fund Method, from the New Energy and Industrial Technology Development Organization (NEDO). TN, KW, TS, AT, MO, TM, and TI are employed by Canon Inc.. TN, TS, TM, KW, TT, YN, YS are the inventors of the indoline derivatives as probe for a biological specimen which has been registered for patent application (WO/2010/074326, WO/2011/077751).

■ ACKNOWLEDGMENTS

We are grateful to Dr. Masahiko Sugimoto (Mie University) for helpful discussion about the advantage of ZMB741 in rodent models, and Masashi Isogai and Ryo Shioda (Perkin-Elmer) for the quantitative assessment of BBB disruption in zebrafish using Volocity. We would also like to thank Reiko Kawase, Hiroko Nakayama, Sayuri Ichikawa, and Michiko Ariyoshi for assistance with the experiments, and Rie Ikeyama and Yuka Tamura for secretarial support.

■ REFERENCES

(1) Neuwelt, E. A., Bauer, B., Fahlke, C., Fricker, G., Iadecola, C., Janigro, D., Leybaert, L., Molnar, Z., O'Donnell, M. E., Povlishock, J. T., Saunders, N. R., Sharp, F., Stanimirovic, D., Watts, R. J., and Drewes, L. R. (2011) Engaging neuroscience to advance translational research in brain barrier biology. *Nat. Rev. Neurosci. 12*, 169−182.

(2) Rosenberg, G. A. (2012) Neurological diseases in relation to the blood-brain barrier. *J. Cereb. Blood Flow Metab.*, 1139−1151.

(3) Shalev, H., Serlin, Y., and Friedman, A. (2009) Breaching the blood-brain barrier as a gate to psychiatric disorder. *Cardiovasc. Psychiatry Neurol. 2009*, 278531.

(4) Kaya, M., and Ahishali, B. (2011) Assessment of permeability in barrier type of endothelium in brain using tracers: Evans blue, sodium fluorescein, and horseradish peroxidase. *Methods Mol. Biol. 763*, 369−382.

(5) Wunder, A., Schoknecht, K., Stanimirovic, D. B., Prager, O., and Chassidim, Y. (2012) Imaging blood-brain barrier dysfunction in animal disease models. *Epilepsia 53* (Suppl6), 14−21.

(6) Le, V. H., and Fishman, W. H. (1947) Combination of Evans blue with plasma protein; its significance in capillary permeability studies, blood dye disappearance curves, and its use as a protein tag. *Am. J. Physiol. 151*, 26−33.

(7) Wolman, M., Klatzo, I., Chui, E., Wilmes, F., Nishimoto, K., Fujiwara, K., and Spatz, M. (1981) Evaluation of the dye-protein tracers in pathophysiology of the blood-brain barrier. *Acta Neuropathol. 54*, 55−61.

(8) Hawkins, B. T., and Egleton, R. D. (2006) Fluorescence imaging of blood-brain barrier disruption. *J. Neurosci. Methods 151*, 262−267.

(9) Nagaraja, T. N., Keenan, K. A., Fenstermacher, J. D., and Knight, R. A. (2008) Acute leakage patterns of fluorescent plasma flow markers after transient focal cerebral ischemia suggest large openings in blood-brain barrier. *Microcirculation 15*, 1−14.

(10) Manaenko, A., Chen, H., Kammer, J., Zhang, J. H., and Tang, J. (2011) Comparison Evans Blue injection routes: Intravenous versus intraperitoneal, for measurement of blood-brain barrier in a mice hemorrhage model. *J. Neurosci. Methods 195*, 206−210.

(11) Benson, R. C., and Kues, H. A. (1978) Fluorescence properties of indocyanine green as related to angiography. *Phys. Med. Biol. 23*, 159−163.

(12) Kim, D. E., Schellingerhout, D., Jaffer, F. A., Weissleder, R., and Tung, C. H. (2005) Near-infrared fluorescent imaging of cerebral thrombi and blood-brain barrier disruption in a mouse model of cerebral venous sinus thrombosis. *J. Cereb. Blood Flow Metab.*, 226−233.

(13) Hoffmann, A., Bredno, J., Wendland, M., Derugin, N., Ohara, P., and Wintermark, M. (2011) High and Low Molecular Weight Fluorescein Isothiocyanate (FITC)-Dextrans to Assess Blood-Brain

Barrier Disruption: Technical Considerations. *Transl. Stroke Res. 2*, 106−111.
(14) Hillman, E. M. (2007) Optical brain imaging *in vivo*: techniques and applications from animal to man. *J. Biomed. Opt. 12*, 051402.
(15) Zhu, D., Wang, Y., Singh, I., Bell, R. D., Deane, R., Zhong, Z., Sagare, A., Winkler, E. A., and Zlokovic, B. V. (2010) Protein S controls hypoxic/ischemic blood-brain barrier disruption through the TAM receptor Tyro3 and sphingosine 1-phosphate receptor. *Blood 115*, 4963−4972.
(16) Yardeni, T., Eckhaus, M., Morris, H. D., Huizing, M., and Hoogstraten-Miller, S. (2011) Retro-orbital injections in mice. *Lab. Anim. (NY) 40*, 155−160.
(17) Jeong, J. Y., Kwon, H. B., Ahn, J. C., Kang, D., Kwon, S. H., Park, J. A., and Kim, K. W. (2008) Functional and developmental analysis of the blood-brain barrier in zebrafish. *Brain Res. Bull. 75*, 619−628.
(18) Xie, J., Farage, E., Sugimoto, M., and Anand-Apte, B. (2010) A novel transgenic zebrafish model for blood-brain and blood-retinal barrier development. *BMC Dev. Biol. 10*, 76.
(19) Watanabe, K., Nishimura, Y., Nomoto, T., Umemoto, N., Zhang, Z., Zhang, B., Kuroyanagi, J., Shimada, Y., Shintou, T., Okano, M., Miyazaki, T., Imamura, T., and Tanaka, T. (2012) *In vivo* assessment of the permeability of the blood-brain barrier and blood-retinal barrier to fluorescent indoline derivatives in zebrafish. *BMC Neurosci. 13*, 101.
(20) Zon, L. I., and Peterson, R. T. (2005) *In vivo* drug discovery in the zebrafish. *Nat. Rev. Drug Discovery 4*, 35−44.
(21) Lawson, N. D., and Wolfe, S. A. (2011) Forward and reverse genetic approaches for the analysis of vertebrate development in the zebrafish. *Dev. Cell 21*, 48−64.
(22) Peterson, R. T., and Macrae, C. A. (2012) Systematic approaches to toxicology in the zebrafish. *Annu. Rev. Pharmacol. Toxicol. 52*, 433−53.
(23) Berezin, M. Y., Guo, K., Akers, W., Livingston, J., Solomon, M., Lee, H., Liang, K., Agee, A., and Achilefu, S. (2011) Rational approach to select small peptide molecular probes labeled with fluorescent cyanine dyes for *in vivo* optical imaging. *Biochemistry. 50*, 2691−2700.
(24) Granger, D. N., Cook, B. H., and Taylor, A. E. (1976) Structural locus of transmucosal albumin efflux in canine ileum. A fluorescent study. *Gastroenterology 71*, 1023−1027.
(25) Alander, J. T., Kaartinen, I., Laakso, A., Patila, T., Spillmann, T., Tuchin, V. V., Venermo, M., and Valisuo, P. (2012) A review of indocyanine green fluorescent imaging in surgery. *Int. J. Biomed. Imaging 2012*, 940585.
(26) Berezin, M. Y., Lee, H., Akers, W., Nikiforovich, G., and Achilefu, S. (2007) Ratiometric analysis of fluorescence lifetime for probing binding sites in albumin with near-infrared fluorescent molecular probes. *Photochem. Photobiol. 83*, 1371−1318.
(27) Peterson, R. T., and Fishman, M. C. (2004) Discovery and use of small molecules for probing biological processes in zebrafish. *Methods Cell Biol. 76*, 569−591.
(28) Padilla, S., Corum, D., Padnos, B., Hunter, D. L., Beam, A., Houck, K. A., Sipes, N., Kleinstreuer, N., Knudsen, T., Dix, D. J., and Reif, D. M. (2012) Zebrafish developmental screening of the ToxCast Phase I chemical library. *Reprod. Toxicol. 33*, 174−187.
(29) Singh, A. K., and P.K., H. (2007) Ethenyl indoles as neutral hydrophobic fluorescence probes. *J. Phys. Org. Chem. 20*, 624−629.
(30) Licha, K., Riefke, B., Ntziachristos, V., Becker, A., Chance, B., and Semmler, W. (2000) Hydrophilic cyanine dyes as contrast agents for near-infrared tumor imaging: synthesis, photophysical properties and spectroscopic *in vivo* characterization. *Photochem. Photobiol. 72*, 392−398.
(31) Freedman, F. B., and Johnson, J. A. (1969) Equilibrium and kinetic properties of the Evans blue-albumin system. *Am. J. Physiol. 216*, 675−681.
(32) Suzuki, Y., and Yokoyama, K. (2005) Design and synthesis of intramolecular charge transfer-based fluorescent reagents for the highly-sensitive detection of proteins. *J. Am. Chem. Soc. 127*, 17799−17802.
(33) Wang, Q., Luo, W., Zheng, W., Liu, Y., Xu, H., Zheng, G., Dai, Z., Zhang, W., Chen, Y., and Chen, J. (2007) Iron supplement prevents lead-induced disruption of the blood-brain barrier during rat development. *Toxicol. Appl. Pharmacol. 219*, 33−41.
(34) Balbuena, P., Li, W., and Ehrich, M. (2011) Assessments of tight junction proteins occludin, claudin 5 and scaffold proteins ZO1 and ZO2 in endothelial cells of the rat blood-brain barrier: cellular responses to neurotoxicants malathion and lead acetate. *Neurotoxicology. 32*, 58−67.
(35) Tuma, R. F., Durán, W. N. and Ley, K. (2008) Microcirculation (Second Edition). Part I: Principles of Microvascular Structure and Function.
(36) Baraban, S. C., Taylor, M. R., Castro, P. A., and Baier, H. (2005) Pentylenetetrazole induced changes in zebrafish behavior, neural activity and c-fos expression. *Neuroscience 131*, 759−768.
(37) Kalayci, R., Kaya, M., Ahishali, B., Arican, N., Elmas, I., and Kucuk, M. (2006) Long-term L-NAME treatment potentiates the blood-brain barrier disruption during pentylenetetrazole-induced seizures in rats. *Life Sci. 79*, 16−20.
(38) Okabe, M., Ikawa, M., Kominami, K., Nakanishi, T., and Nishimune, Y. (1997) "Green mice" as a source of ubiquitous green cells. *FEBS Lett. 407*, 313−319.
(39) Cai, M., Phan, P. T., Hong, J. G., Kim, D. H., Kim, J. M., Park, S. J., Liu, X., Han, J. E., Park, H., Choi, J. W., and Ryu, J. H. (2012) The neuroprotective effect of eupatilin against ischemia/reperfusion-induced delayed neuronal damage in mice. *Eur. J. Pharmacol. 689*, 104−110.
(40) Jin, A. Y., Tuor, U. I., Rushforth, D., Kaur, J., Muller, R. N., Petterson, J. L., Boutry, S., and Barber, P. A. (2010) Reduced blood brain barrier breakdown in P-selectin deficient mice following transient ischemic stroke: a future therapeutic target for treatment of stroke. *BMC Neurosci. 11*, 12.
(41) Beck, J., Stummer, W., Lehmberg, J., Baethmann, A., and Uhl, E. (2007) Activation of leukocyte-endothelial interactions and reduction of selective neuronal death after global cerebral ischemia. *Neurosci. Lett. 414*, 159−164.
(42) Yata, K., Mizoguchi, A., Shindo, A. and Tomimoto, H. (2010) Assessment of cerebral blood flow in a mouse model of chronic cerebral hypoperfusion using two-photon laser scanning microscopy. In *51st Annual Meeting of the Japanese Society of Neurology*, Tokyo, Japan.
(43) Bertram, K. J., Shipley, M. T., Ennis, M., Sanberg, P. R., and Norman, A. B. (1994) Permeability of the blood-brain barrier within rat intrastriatal transplants assessed by simultaneous systemic injection of horseradish peroxidase and Evans blue dye. *Exp. Neurol. 127*, 245−252.
(44) O'Malley, D. M., Sankrithi, N. S., Borla, M. A., Parker, S., Banden, S., Gahtan, E., and Detrich, H. W., 3rd. (2004) Optical physiology and locomotor behaviors of wild-type and nacre zebrafish. *Methods Cell Biol. 76*, 261−284.
(45) Parichy, D. M., Mellgren, E. M., Rawls, J. F., Lopes, S. S., Kelsh, R. N., and Johnson, S. L. (2000) Mutational analysis of endothelin receptor b1 (rose) during neural crest and pigment pattern development in the zebrafish Danio rerio. *Dev. Biol. 227*, 294−306.
(46) Westerfield, M. (2007) *A guide for the laboratory use of zebrafish (Danio rerio)*, University of Oregon Press, Eugene, OR.
(47) Schwartz, A., Wang, L., Early, E., Gaigalas, A., Zhang, Y., Marti, G. E., and Vogt, R. F. (2002) Quantitating fluorescence intensity from fluorophore: the definition of MESF assignment. *J. Res. Natl. Inst. Stand. Technol. 107*, 339−353.
(48) Turro, N. (1991) *Modern Molecular Photochemistry*, pp 109−110 and 187−188, University Science Books, Mill Valley, CA.
(49) Watanabe, K., Nishimura, Y., Oka, T., Nomoto, T., Kon, T., Shintou, T., Hirano, M., Shimada, Y., Umemoto, N., Kuroyanagi, J., Wang, Z., Zhang, Z., Nishimura, N., Miyazaki, T., Imamura, T., and Tanaka, T. (2010) *In vivo* imaging of zebrafish retinal cells using fluorescent coumarin derivatives. *BMC Neurosci. 11*, 116.

(50) Yang, G., Pan, F., Parkhurst, C. N., Grutzendler, J., and Gan, W. B. (2010) Thinned-skull cranial window technique for long-term imaging of the cortex in live mice. *Nat. Protoc. 5*, 201−208.